

Precise Enumeration of Circulating Tumor Cells Using Support Vector Machine Algorithm on a Microfluidic Sensor

JINHONG GUO^{1,2}, ZHI CHEN¹, YONG-LING BAN³, AND YUEJUN KANG²

¹National Key Laboratory of Science and Technology on Communications, University of Electronic Science and Technology of China, Chengdu 611731, China

²School of Chemical and Biomedical Engineering, Nanyang Technological University, Singapore 637459

³Institute of Electromagnetics, University of Electronic Science and Technology of China, Chengdu 611731, China

CORRESPONDING AUTHOR: Y. KANG (yuejun.kang@ntu.edu.sg)

The work of Y. Kang was supported in part by a Sustainable Earth Office Award through the Nanyang Technological University and in part by a Tier-1 Academic Research Fund through the Ministry of Education of Singapore, Singapore, under Grant RG 26/11. The work of J. Guo and Z. Chen was supported in part by the National Higher-Education Institution General Research and Development Project under Grant ZYGX2013J013 and in part by the National Science and Technology Specific Projects of China under Grant 2013ZX03001024.

ABSTRACT Smart hospital is believed to be a promising technology and platform that could tremendously improve healthcare in the future. This technology is featured by a front sensor to collect the relevant biomedical data to help the doctor analyze the patient's condition and make diagnostic decisions. Precise analysis of these data is critical to improve the reliability of diagnostic methods. In this paper, we demonstrate a microfluidic impedance cytometer based on a solid-state micropore for the detection and enumeration of cancer cells from the red blood cells. The two important parameters of the signal pulses, including the peak amplitude and the pulse bandwidth, were analyzed by the support vector machine (SVM) algorithm to classify all the cell events into two different subpopulations accurately. The proposed microfluidic sensor combined with the SVM algorithm can provide a promising platform, which may be used for construction of sensor network in smart hospital.

INDEX TERMS Smart hospital, robust diagnosis, microfluidic, impedance, micropore, support vector machine.

I. INTRODUCTION

Smart hospital is defined as information-based infrastructure which incorporates functions of sensing, actuation and control above the traditional hospital. It is capable of describing and analyzing the disease, and taking decisions based on the available data in a predictive or adaptive manner, thereby performing smart actions. Sensor plays a significant role in the data collection part. Coulter Counter (also known as impedance cytometry) has emerged as a powerful tool for detection and enumeration of biological particles or cells suspended in electrolyte solution [1]. Their applications range widely from analysis of pollen [2], human cells [3], bacteria [4], viruses [5], DNA and other biomolecules [6]–[8], to metal ion detection for some industrial and environmental applications. When microparticles or cells translocate through a micro/nano sensing aperture, the aperture is

electrically blocked because these non-conducting particles displace the conducting electrolyte solution [9]. This results in the significant electrical current change across the aperture. By analyzing the change of electrical pulse amplitude and pulse bandwidth, the information of size and numbers of the microparticles can be obtained. Recently, due to the fast development of micro/nanofabrication technology, micro-Coulter counter have been developed for point-of-care analysis of whole blood cells and cancer cells at low cost [10]–[16]. It is well known that circulating tumor cells (CTCs) can be detected in the blood circulation of most cancer patients in spite of their extremely low concentration. Precise enumeration of CTCs in the circulating blood is believed to be critical for monitoring disease progression and assessing the patient response to treatment. The conventional flow cytometry technique that is based on the fluorescent tag is limited due to

high operation cost and bulky instruments. In contrast, the microfluidic impedance cytometry can provide a rapid and cost-effective solution for characterization of tumor cells. In addition, due to the excellent portability of the microfluidic impedance cytometer, it can be used as a front sensor terminal to collect patient information, and transfer the data remotely through a sensor network as in the future smart hospital.

In this paper, we develop a microfluidic sensor with a solid-state micropore fabricated inside a silicon wafer. The proposed chip is calibrated by the polystyrene microparticles of standard sizes. Mixed samples with red blood cells and tumor cells are measured and processed by the support vector machine (SVM) algorithm. It can be demonstrated that this microfluidic sensor with such signal processing algorithm is capable of providing precise enumeration of the tumor cells, which has a great potential in construction of sensor network for future smart hospital.

II. THEORY AND METHOD

A. NUMERICAL MODELING

The pulse peak amplitude and pulse bandwidth are two critical parameters to differentiate the particles/cells with different phenotypes. The pulse peak amplitude induced by micro-particles can be analytically derived, while the pulse bandwidth can be evaluated by numerical method, as shown in the following.

1) PULSE PEAK AMPLITUDE

When the particle passes through the narrow sensing micropore, it will induce a significant modulation on the micropore resistance, because its comparable size causes partial blockage of the aperture. We assume ΔR is the resistance change due to the transient presence of a particle in the micropore. The electric currents through the sensing aperture without particle can be expressed as:

$$I = \frac{V_{in}}{R_{in}} \quad (1)$$

where V_{in} is the total bias across the main channel. The electrical current change ΔI is induced by the small resistance change of the micropore and can be derived as:

$$\frac{\Delta I}{\Delta R} \approx \frac{dI}{dR} = -\frac{V_{in}}{R_{in}^2} \quad (2)$$

Consequently, the change in electrical resistance can be written as:

$$|\Delta I| \approx \frac{V_{in}}{R_{in}^2} \cdot \Delta R \quad (3)$$

On the other hand, the resistance change can be approximated by the formula derived by Gregg and Steidley [17]:

$$\Delta R \approx -\frac{\rho V}{\pi^2 r_m^4} \left(\frac{1 + 0.3K^2 + 0.13K^4 + \dots}{\sqrt{1 - K^2}} \right) \quad (4)$$

where V is the particle volume and K is the diameter ratio between the particle and the aperture. When $K \ll 1$, the

resistance change is linearly proportional to the particle volume. However, when the particle size is comparable to the aperture size, the relationship between the resistance change and particle volume becomes non-linear and hence higher order terms of K in Eq. (4) need to be considered when evaluating the resistance change induced by comparable particle in dimension.

2) PULSE BANDWIDTH

A 3-dimensional model is developed using commercial Finite Element Method software COMSOL Multiphysics® 4.3 (COMSOL, CA, USA). During the simulation, the particle is released at a near aperture upstream location before it enters the sensing aperture. The carrying liquid flow is driven by the inlet flow at the entry of the channel, which exerts hydrodynamic force on the particle. The particle also experiences the electrophoretic and dielectrophoretic forces due to the electrical potential applied over the conducting liquid channel. In order to characterize the pulse profile resulted from particle translocation, the electrical field, and the flow field, all governing equations need to be coupled together in computation: [10], [11], [16].

Navier-Stokes equation for the fluid flow:

$$\rho \left[\frac{\partial \vec{u}}{\partial t} + \vec{u} \cdot \nabla \vec{u} \right] = -\nabla p + \mu \nabla^2 \vec{u} \quad (5)$$

Continuity equation:

$$\nabla \cdot \vec{u} = 0 \quad (6)$$

Boundary conditions [14]:

Channel walls:

$$\vec{u} = -\frac{\varepsilon_0 \varepsilon_r \zeta_w}{\mu} \vec{E}, \vec{n} \cdot \nabla p = 0 \quad (7a)$$

Particle surface:

$$\vec{u} = \vec{V}_p - \frac{\varepsilon_0 \varepsilon_r \zeta_p}{\mu} \vec{E}, \vec{n} \cdot \nabla p = 0 \quad (7b)$$

Inlet:

$$\vec{n} \cdot \nabla \vec{u} = 0, v_{inlet} = v_0 \quad (7c)$$

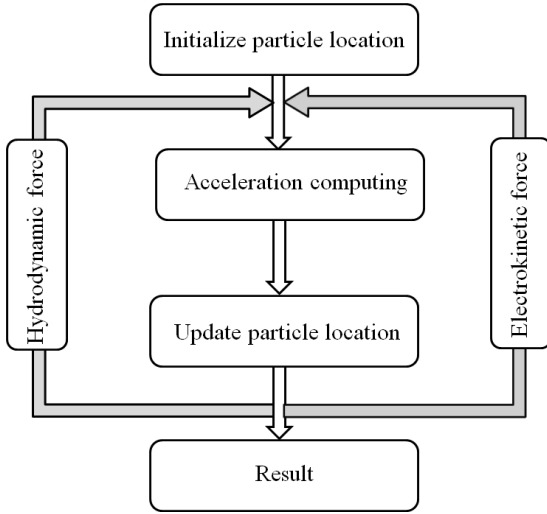
Outlet:

$$\vec{n} \cdot \nabla \vec{u} = 0, p = 0 \quad (7d)$$

where \vec{u} is flow velocity; v_0 denotes the inlet flow rate; ρ is the fluid density; μ is the dynamic viscosity; ζ_p is the zeta potential at particle surface and ζ_w is the zeta potential at the channel wall; \vec{E} is the electrical field and \vec{V}_p is translational velocity of the particle. The governing equation of particle motion is described by Newton's second law:

$$\vec{m}_p \frac{d\vec{V}_p}{dt} = \vec{F}_{net} \quad (8)$$

where m_p is the mass of the particle, \vec{F}_{net} is the net force exerting on the particle. The net force consists of two forces: electrophoretic force \vec{F}_{DEP} due to the applied electrical field



Scheme 1. Simulation flow diagram.

and the hydrodynamic force \vec{F}_{ho} due to the carrying flow field. Therefore, the total net force is given as

$$\vec{F}_{net} = \vec{F}_{DEP} + \vec{F}_{ho} \quad (9)$$

Since the electric field is computed in the model, the dielectrophoretic force can be defined by Maxwell stress tensor:

$$F_{DEP} = \oint_S \bar{\bar{T}} \cdot \vec{n} dS \quad (10)$$

where $\bar{\bar{T}}$ is the Maxwell stress tensor and can be written as:

$$\bar{\bar{T}} = \varepsilon(E \otimes E - \frac{1}{2}E^2I) \quad (11)$$

where I is the unit tensor and \otimes denotes the dyadic product.

The hydrodynamic force in the outer region is described by integrating fluidic tensor over the particle surface [10], [11]:

$$\vec{F}_{ho} = - \oint_S \bar{\bar{\sigma}}_p \cdot \vec{n} dS \quad (12)$$

where S is the particle surface, $\bar{\bar{\sigma}}_p$ is the stress tensor given by [16]

$$\bar{\bar{\sigma}}_p = -p\bar{\bar{I}} + \mu[\nabla\vec{u} + (\nabla\vec{u})^T] \quad (13)$$

For simplicity, the initial condition of particle motion is set to zero:

$$\vec{V}_p|_{t=0} = 0, \quad \vec{u}|_{t=0} = 0 \quad (14)$$

An adaptive mesh set was applied to the model. The ultra-fine mesh was applied for the aperture while the fine mesh was employed for other parts. The maximum mesh size is $5 \mu\text{m}$, and the minimum mesh size is $0.1 \mu\text{m}$. The total number of mesh units is 1.28 million. The simulation flow diagram is indicated in the following scheme. Detailed dimension for the channel structure is listed in Table I.

TABLE 1. The dimension of the microstructure.

	Diameter	Depth
Upper chamber	1 mm	1 mm
Aperture	20 μm	30 μm
Backside hole	400 μm	300 μm

3) DATA ANALYSIS ALGORITHM

The peak amplitude and bandwidth of the recorded signals were collected through a home-made program developed using MATLAB (Mathworks, MA, USA). A signal processing method based on support vector machine (SVM) was used to classify the measured cell events in order to distinguish the different sub-populations. SVM is a promising alternative way as compared to artificial neural network (ANN) for classifying impedance data for different cell populations. However, ANN is limited by some disadvantages such as network configuration complexity. The principle of SVM is to train a model with the given inputs x_i (e.g., the amplitude value of the current spike or other impedance relevant parameters) and the given output y_i (two classes such as 1 or -1) by solving the following optimization problem:

$$\begin{aligned} \min_{\omega, b, \xi} \quad & \frac{1}{2}\omega^T \omega + C \sum_{i=1}^l \xi_i \\ \text{subject} \quad & y_i(\omega^T \phi(x_i) + b) \geq 1 - \xi_i, \xi_i \geq 0, i = 1, \dots, l, \end{aligned} \quad (15)$$

where $\phi(x_i)$ maps x_i into a higher dimensional space and $C > 0$ is the regularization parameter. Due to the possible high dimensionality of ω , we solve the following dual problem instead of the original Eq.(15).

$$\begin{aligned} \min_{\omega, b, \xi} \quad & \frac{1}{2}\omega^T \omega + C \sum_{i=1}^l \xi_i \\ \text{subject} \quad & y_i(\omega^T \phi(x_i) + b) \geq 1 - \xi_i, \xi_i \geq 0, i = 1, \dots, l, \end{aligned} \quad (16)$$

where $e = [1, 1, \dots, 1]^T$ and Q is a positive semi-definite matrix, $Q = y_i y_j K(x_i, x_j)$ and $K = \phi(x_i)^T \phi(x_j)$ is the kernel function. Radial basis function (RBF) is appointed as the kernel function in this study. After Eq. (16) is solved, the optimal ω satisfies:

$$\omega = \sum_{i=1}^l y_i \alpha_i \phi(x_i) \quad (17)$$

And the design function is used to classify the outputs:

$$\text{sgn}(\omega^T \phi(x) + b) = \text{sgn}\left(\sum_{i=1}^l y_i \alpha_i K(x_i, x) + b\right) \quad (18)$$

In practice, the SVM-based signal processing algorithm was implemented and used as follows: (1) we first took two impedance measurements separately using different samples (e.g., red blood cells vs. tumor cells) to generate the training and validated model, where both inputs (the measured signal) and outputs (the classification of the sample, e.g., 1 for red blood cell and -1 for tumor cell) were known; (2) the training and validation model was used to train the SVM classification

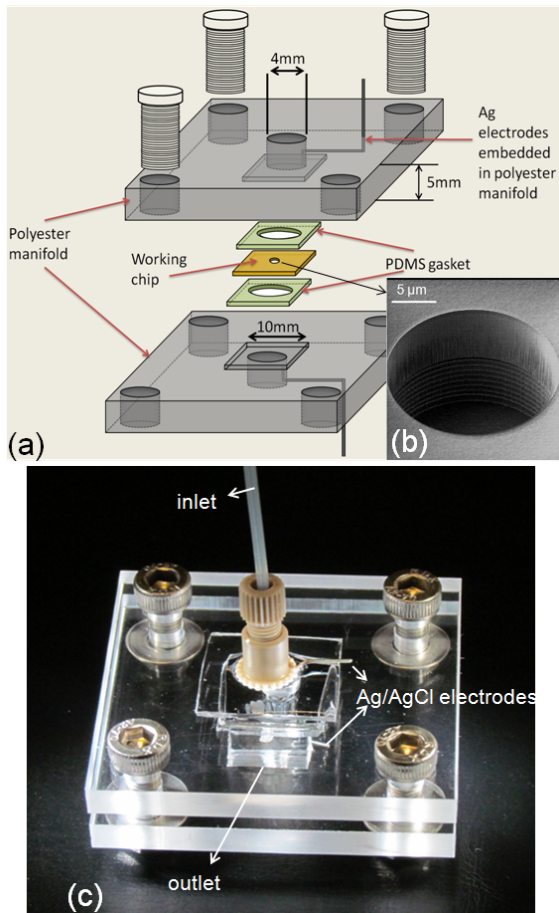


Fig. 1. (a) The schematic view of proposed impedance cytometer; (b) the etched solid state micropore under SEM; (c) the packaged device with two inserted electrodes.

mechanism and investigates its accuracy, respectively; and (3) a test using the mixed sample of both cells (tumor cells and red blood cells) was performed, where only inputs were known while outputs were unknown. The output values using the trained SVM mechanism, i.e., classifying all the data into the corresponding contents is determined. The SVM library was utilized in the algorithm development [18]. The algorithm was developed using MATLAB.

B. SENSOR CONFIGURATION AND FABRICATION

The microfluidic sensor comprises a micropore on a silicon wafer, and a plastic package. As Fig. 1 shows, the dimension of the micropore is $20\ \mu\text{m}$ in diameter and $30\ \mu\text{m}$ in length. Two PDMS gaskets are used to clamp the silicon chip. The dimension of the whole device is $5\text{cm} \times 5\text{cm}$.

The proposed device was fabricated on an 8 inch silicon wafer, which was pre-deposited with $20\ \mu\text{m}$ SiO_2 as the dielectric layer. There were three lithographic steps. The first step was to etch a micropore of $20\ \mu\text{m}$ in diameter from the top side. After spin coating with a $2\ \mu\text{m}$ thick thin film photoresist (UV26-2.5, Dow Chemicals, Singapore), the device was exposed to ultraviolet (UV) light to open the etching area. Reactive ion etching (RIE) was used to etch the $20\ \mu\text{m}$

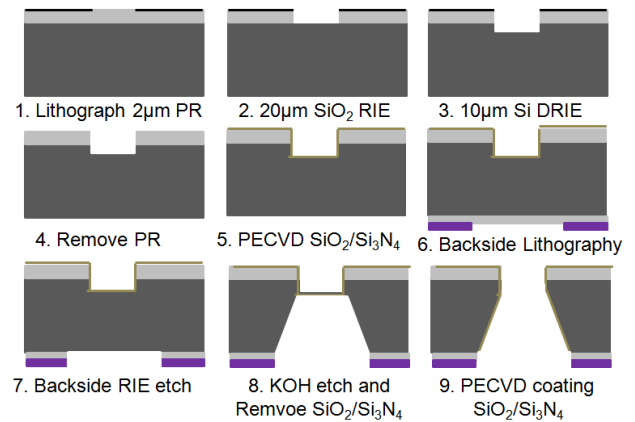


Fig. 2. The fabrication procedures of the solid-state micropore on a silicon wafer.

dielectrics of the chip and deep RIE (DRIE) was used to further etch $10\ \mu\text{m}$ into silicon. After etching, photoresist was removed and the wafer was cleaned. Then the wafer was deposited with $100\ \text{nm}$ SiO_2 and $150\ \text{nm}$ of Si_3N_4 using plasma-enhanced chemical vapor deposition (PECVD) as a protection layer for the subsequent processing. The wafer was thinned down to around $400\ \mu\text{m}$ by back grinding. The second lithography was used to etch the pore from the back side of the wafer. $\text{SiO}_2/\text{Si}_3\text{N}_4$ were deposited on the backside as hard mask for the back side etching. After photoresist coating and UV exposure from the backside, RIE was used to etch the $\text{SiO}_2/\text{Si}_3\text{N}_4$ hard mask to expose the silicon, followed by wet etching of silicon using KOH. Then the remaining $\text{SiO}_2/\text{Si}_3\text{N}_4$ protection layer for the front side, which blocked the pore, was removed by buffered oxide etching (BOE) and H_3PO_4 etching. Finally, the whole wafer, including the interior side of the pore, was coated with $\text{SiO}_2/\text{Si}_3\text{N}_4$. The wafer was diced and ready for the testing. Fig. 2 shows the schematics of the fabrication procedure and a SEM image of the etched micropore.

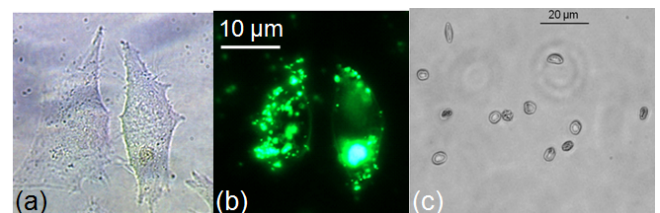


Fig. 3. (a) The HeLa cells under an optical microscope. (b) The HeLa cells stained with DAPI under a fluorescent microscope. (c) The suspended red blood cells under a optical microscope.

C. CELLS PREPARATION

HeLa cells (American Type Culture Collection, MD, USA) were cultured in Dulbecco's Modified Eagle Medium (DMEM) supplemented with 10% fetal bovine serum (FBS), 1 mM sodium pyruvate, 0.1 mM MEM nonessential amino acids. The cells were grown at $37\ ^\circ\text{C}$ under a 5% CO_2 in a T75 flask. Fig. 3 shows the contrast and fluorescent images of

the HeLa cells to be tested. The whole blood was centrifuged at 2000 g for 15 min. The RBCs were obtained at the bottom of the centrifuge tube. Then the RBCs were re-suspended in fresh PBS in a new tube.

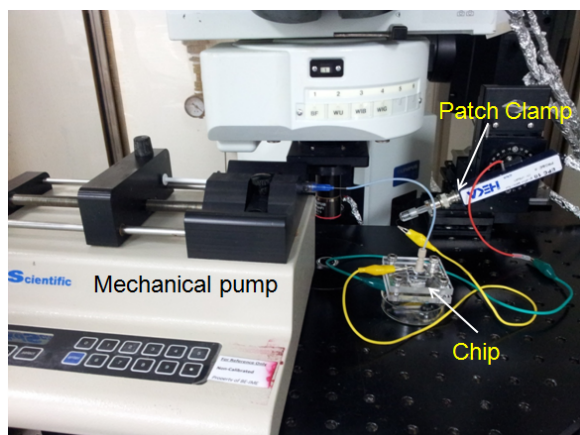


Fig. 4. The system setup for the experiment.

D. EXPERIMENTAL SETUP

Fig. 4 shows the typical setup of the experiment. The device has two Ag/AgCl electrodes connected to the measurement system. The samples were injected from inlet reservoir and the waste was removed from the outlet reservoir loaded at the bottom chamber. A syringe pump was used to perfuse the sample flow through the main channel at a flow rate of $5 \mu\text{L}/\text{min}$. The electrical current across the micropore was measured under a total bias of 1 V across the main channel by using a patch clamp amplifier (EPC10 USB Quadro, HEKA Elektronik, Lambrecht, Germany), which provided accurate detection of the tiny current modulation with high signal-to-noise ratio. The data were collected at sampling rate of 100 kHz and imported into a MATLAB program for post-processing.

III. RESULTS AND DISCUSSION

A. DETECTION OF POLYSTYRENE MICROPARTICLES

As discussed in the theoretical analysis, the current change due to the blockage of the particle is linearly proportional to the particle volume. To calibrate the device performance and optimize the working condition, we used polystyrene particles of various sizes ($7\mu\text{m}$, $10\mu\text{m}$ and $16\mu\text{m}$) as target samples. Fig. 5a indicates a series of detected peaks induced by the three types of polystyrene particles. It is obvious that larger particles induce greater current change. A good linearity with regression ($R^2 = 0.998$) was obtained by comparing the peak amplitude (%) with the volume of the microparticles (Fig. 5b). Fig. 5c indicates the pulse bandwidth induced by the polystyrene particles of different sizes. The experimental results show a good agreement with the simulation results for both peak amplitude and pulse bandwidth within the acceptable error range. We speculate that the greater discrepancy of the peak amplitude data for large particle ($16\mu\text{m}$) is due to the

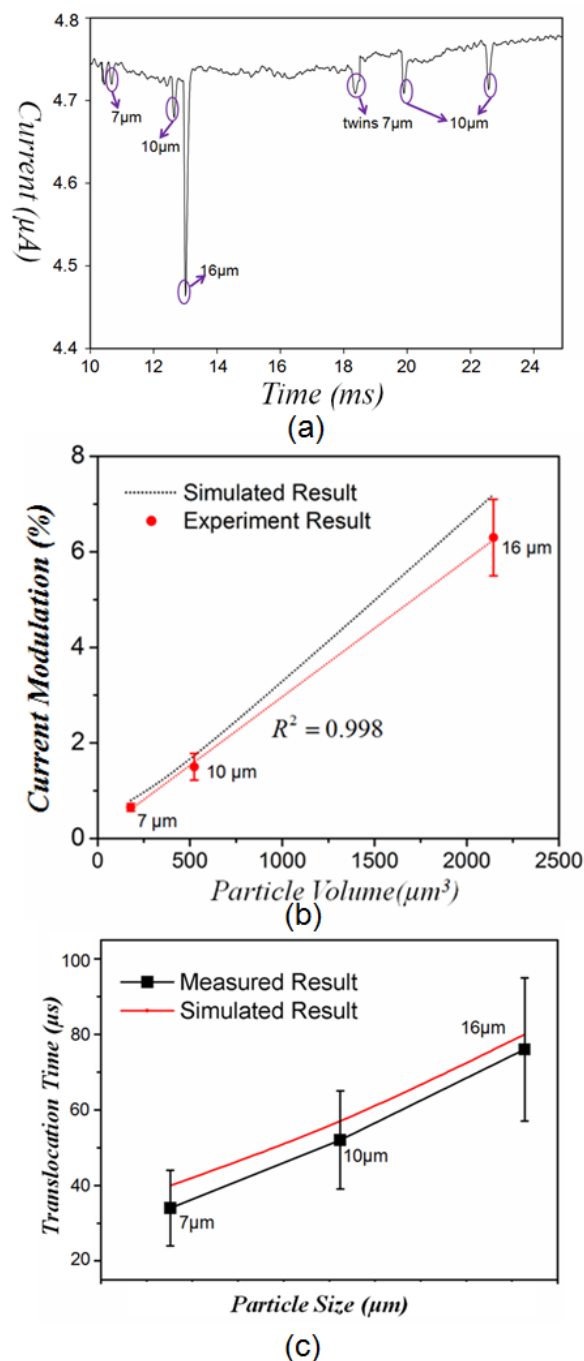


Fig. 5. (a) The electric current variation due to the electrical blockage of $7 \mu\text{m}$, $10 \mu\text{m}$ and $16 \mu\text{m}$ polystyrene particles; (b) comparison between the simulation and experimental results of the electric current modulation in percentage induced by $7 \mu\text{m}$, $10 \mu\text{m}$, and $16 \mu\text{m}$ polystyrene particles. (c) comparison between the simulated and experimental results of pulse bandwidth induced by $7 \mu\text{m}$, $10 \mu\text{m}$, and $16 \mu\text{m}$ polystyrene particles.

off-center axis motion of the particle [19], which has not been taken into account in our numerical simulation. It is implied that the measured data of microparticles with different size can be differentiated by correlation analysis of pulse peak amplitude and pulse bandwidth.

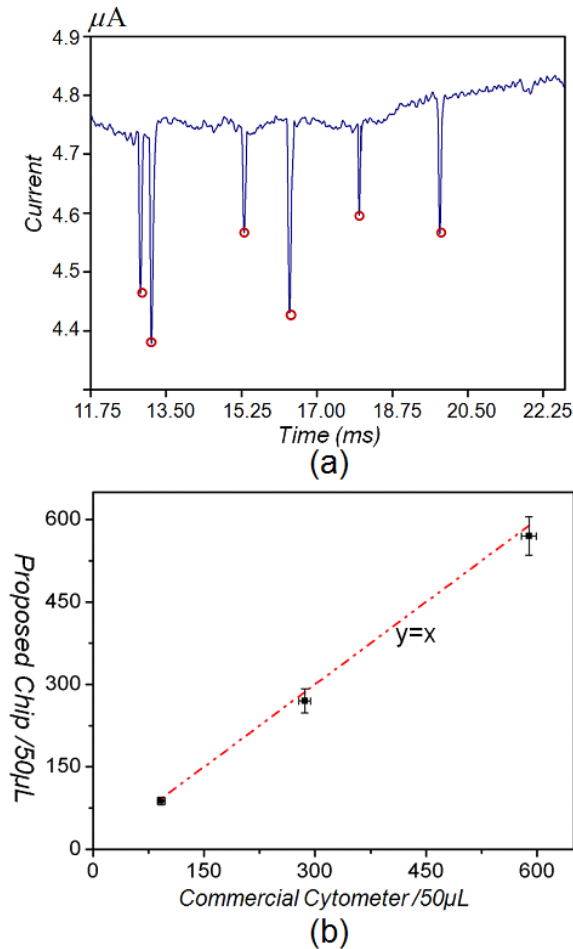


Fig. 6. (a) Continuously monitor the tumor cells by the chip, each spike indicate one tumor cell; (b) Hela cells enumeration by both commercial cytometer and the proposed chip with a good agreement between these two methods.

B. ENUMERATION OF CIRCULATION TUMOR CELLS

In order to investigate the accuracy of the device for enumeration of tumor cells, specific concentration (in the ranges of $2 \times 10^3 \text{ mL}^{-1}$, $6 \times 10^3 \text{ mL}^{-1}$ and $1.2 \times 10^4 \text{ mL}^{-1}$, respectively) of Hela cells were tested by both the microfluidic sensor and a commercial cytometer (FC500, Beckman Coulter, CA, USA). Fig. 6a shows the continuously monitoring of typical current pulses induced by Hela cells, in which each downward spike represents a single tumor cell event and the amplitude of the pulse is proportional to volume (i.e., size) of the cell. Fig. 6b demonstrates the excellent accuracy of the microfluidic sensor as compared to a commercial cytometer, for all three samples with different cell concentrations.

C. TEST OF TUMOR CELLS AND RED BLOOD CELLS

The translocation time of a single cell, by characterizing the modulated pulse bandwidth, could be another important parameter in analyzing the biological cells using Coulter principle, because it is an indicative parameter related to other cellular physiological characteristics. For example, if one cell

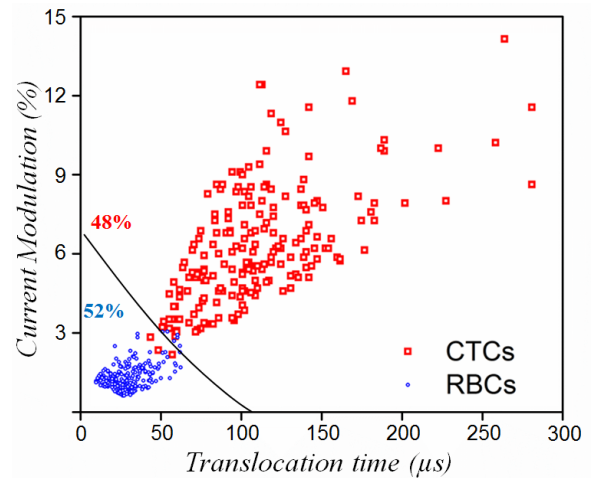


Fig. 7. The scattered dot plot in terms of the peak amplitude and translocation time for RBCs and tumor cells, measured in different suspension.

deforms when it squeezes through a small aperture due to the geometrical constriction or the flow shear stress, it becomes longer in shape in the direction of the flow (spheroidal shape), which will effectively increase the translocation time. There is recent evidence indicating that the tumor cells have much higher flexibility and tend to deform more easily compared to other cell types, which could facilitate the tumor cells to penetrate the endothelial barriers and cause metastasis [20], [21]. Hence the translocation time could be another important parameter to measure the cell deformability that may help further differentiate the tumor cells from other blood cells. Consequently, the correlation spectroscopy by two parameters, pulse amplitude and the pulse bandwidth, can be concurrently analyzed for determination of different cell types. In order to generate the training and validation data for support vector machine algorithm, RBCs and tumor cells were both tested by the proposed device, respectively. The two samples containing RBCs of 7500 cells/ml and CTCs of 6000 cells/ml, respectively, were spiked in 1X PBS solution. The applied DC bias on the chip was 1 V. Totally about 523 cell events, including RBCs and CTCs, were measured and analyzed (Fig. 7). As discussed earlier, the RBCs induce smaller peak amplitude than the CTCs, because the tumor cells have larger size resulting in a greater blockage of the sensing aperture. Fig. 7 shows obvious contrast between these two distinct groups of cells in the correlation between peak amplitude and translocation time. The signal processing based on SVM was used to define a classification boundary for resolving the distinct sub-populations.

D. CLASSIFICATION OF TUMOR CELLS MIXED WITH RED BLOOD CELLS

The sample containing RBCs of 7500 cells/ml and tumor cells of 4200 cells/ml were mixed and spiked in 1X PBS solution. This mixture was further split into two equal aliquots to be tested by the microfluidic sensor and a commercial

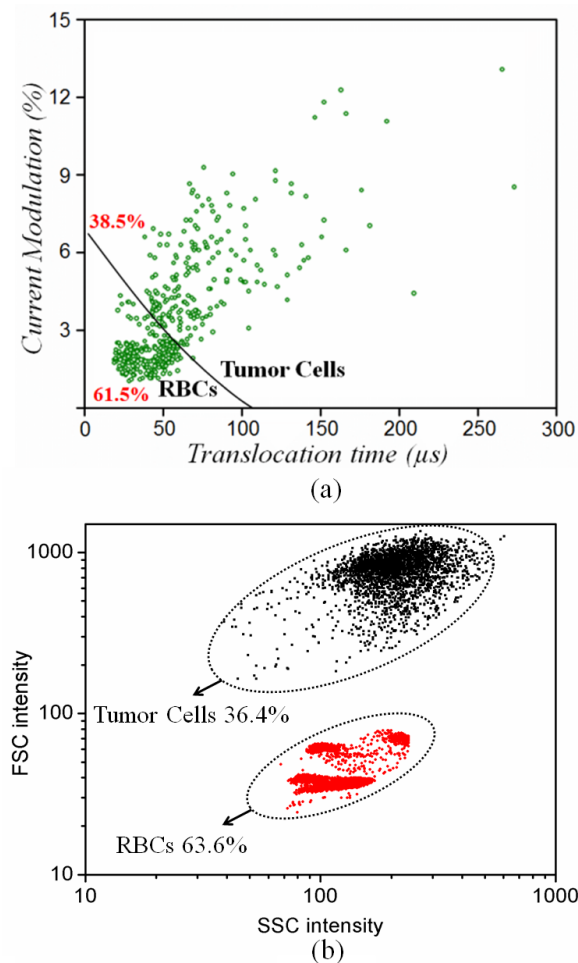


Fig. 8. Result comparison for mixed RBCs and tumor cells: (a) The scattered dot plot in terms of impedance peak amplitude and translocation time measured by microfluidic chip; (b) The scattered dot plot in terms of forward scatter (FSC) and side scatter (SSC) measured by commercial flow cytometer.

flow cytometer (Beckman-Coulter[®] FC500), respectively. Under the same experimental condition as in section 3.3, totally about 600 cell events were measured and analyzed (Fig. 8a) by the microfluidic sensor. Based on the classification boundary obtained from the training results in Fig. 7, we can evaluate the sub-populations of tumor cells, which are located above the classification boundary. Fig. 8a indicated that out of the 600 detected events, 231 tumor cells were detected by the proposed device and the other 369 events were judged as the red blood cells. With three independent test running, the developed impedance cytometer obtained the tumor cell percentage as $38.2\% \pm 2\%$, while the commercial flow cytometry obtained a corresponding percentage of $36.4\% \pm 0.5\%$. These results implied that this impedance cytometer can potentially provide a solution for relatively reliable and low cost platform for the tumor cell detection from circulating blood cells.

It was noted that the boundary between these two types of cells in the mixed samples (Fig. 8a) is less clear compared to

that in the individual training test (Fig. 7). We speculate that there could be two reasons: firstly, the flow rate for mixed/unmixed samples might be slightly different, which cause the systematic shift in the data for translocation time; secondly, some of the tumor cells shrank during the mixing procedure, which might be due to the slightly increased tonicity of the PBS solution. This finding suggests that the working conditions, including the flow rate and solute tonicity, have to match very well between the training and actual test in order to accurately calibrate this microfluidic impedance cytometer.

IV. CONCLUSION

In this proof-of-concept study, we developed a microfluidic sensor with a solid-state micropore fabricated on a silicon wafer, which can provide precise detection of tumor cells from red blood cells using signal processing algorithm based on support vector machine (SVM). This method can generate highly accurate data, thereby facilitating more reliable clinical diagnostics. In summary, the proposed microfluidic sensor combined with SVM is of great potential for the biomedical application in the smart hospital near the future.

REFERENCES

- [1] Y.-N. Wang et al., "On-chip counting the number and the percentage of CD4+ T lymphocytes," *Lab Chip*, vol. 8, no. 2, pp. 309–315, 2008.
- [2] S. Zheng, M. Liu, and Y. C. Tai, "Micro coulter counters with platinum black electroplated electrodes for human blood cell sensing," *Biomed. Microdevice*, vol. 10, no. 2, pp. 221–231, 2008.
- [3] Y. Zheng, J. Nguyen, C. Wang, and Y. Sun, "Electrical measurement of red blood cell deformability on a microfluidic device," *Lab Chip*, vol. 13, no. 16, pp. 3275–3283, 2013.
- [4] E. M. Swanton, W. A. Curby, and H. E. Lind, "Experiences with the Coulter counter in bacteriology," *Appl. Microbiol.*, vol. 10, no. 5, pp. 480–485, 1962.
- [5] G. Damhorst, B. M. Venkatesan, S. Banerjee, V. Solovyeva, and R. Bashir, "A submicron coulter counter for enumeration of viruses and nanoparticles," *Biophys. J.*, vol. 102, no. 3, p. 584a, 2012.
- [6] L. J. Steinbock, O. Otto, C. Chimere, J. Gornall, and U. F. Keyser, "Detecting DNA folding with nanocapillaries," *Nano Lett.*, vol. 10, no. 7, pp. 2493–2497, 2010.
- [7] H. Bayley and C. R. Martin, "Resistive-pulse sensing—from microbes to molecules," *Chem. Rev.*, vol. 100, no. 7, pp. 2575–2594, 2000.
- [8] C. Dekker, "Solid-state nanopores," *Nature Nanotechnol.*, vol. 2, pp. 209–215, Mar. 2007.
- [9] K. H. Kang, Y. Kang, X. Xuan, and D. Li, "Continuous separation of microparticles by size with direct current-dielectrophoresis," *Electrophoresis*, vol. 27, no. 3, pp. 694–702, 2006.
- [10] J. Guo, T. S. Pui, Y.-L. Ban, A. R. A. Rahman, and Y. Kang, "Electrokinetic analysis of cell translocation in low-cost microfluidic cytometry for tumor cell detection and enumeration," *IEEE Trans. Biomed. Eng.*, vol. 60, no. 12, pp. 3269–3275, Dec. 2013.
- [11] J. Guo, W. Lei, X. Ma, P. Xue, Y. Chen, and Y. Kang, "Design of a fluidic circuit-based microcytometer for circulating tumor cell detection and enumeration," *IEEE Trans. Biomed. Circuits Syst.*, vol. 8, no. 1, pp. 35–41, Feb. 2014.
- [12] W. Asghar, Y. Wan, A. Ilyas, R. Bachoo, Y.-T. Kim, and S. M. Iqbal, "Electrical fingerprinting, 3D profiling and detection of tumor cells with solid-state micropores," *Lab Chip*, vol. 12, no. 13, pp. 2345–2352, 2012.
- [13] Y. Wu, J. D. Benson, and M. Almasri, "Micromachined Coulter counter for dynamic impedance study of time sensitive cells," *Biomed. Microdevice*, vol. 14, no. 4, pp. 739–750, 2012.
- [14] J. I. Zwicker, "Impedance-based flow cytometry for the measurement of microparticles," *Semin Thromb Hemost.*, vol. 36, no. 8, pp. 819–823, 2010.
- [15] H. Choi et al., "A label-free DC impedance-based microcytometer for circulating rare cancer cell counting," *Lab Chip*, vol. 13, no. 5, pp. 970–977, 2013.

- [16] J. Guo, T. S. Pui, A. R. R. Rahman, and Y. Kang, "3D numerical simulation of a Coulter counter array with analysis of electrokinetic forces," *Electrophoresis*, vol. 34, no. 3, pp. 417–424, 2013.
- [17] E. C. Gregg and K. D. Steidley, "Electrical counting and sizing of mammalian cells in suspension," *Biophys. J.*, vol. 5, no. 4, pp. 393–405, 1965.
- [18] (2013, Oct. 3). *LIBSVM—A Library for Support Vector Machines*. [Online]. Available: <http://www.csie.ntu.edu.tw/~cjlin/libsvm/>
- [19] Z. Qin, J. Zhe, and G.-X. Wang, "Effects of particle's off-axis position, shape, orientation and entry position on resistance changes of micro Coulter counting devices," *Meas. Sci. Technol.*, vol. 22, no. 4, p. 045804, 2011.
- [20] W. Xu, R. Mezencev, B. Kim, L. Wang, J. McDonald, and T. Sulcheck, "Cell stiffness is a biomarker of the metastatic potential of ovarian cancer cells," *PLOS ONE*, vol. 7, no. 10, p. e46609, 2012.
- [21] S. Byun et al., "Characterizing deformability and surface friction of cancer cells," *Proc. Nat. Acad. Sci. United States Amer.*, vol. 110, no. 19, pp. 7580–7585, 2013.



JINHONG GUO received the B.E. degree in electronic engineering from the University of Electronic Science and Technology of China, Chengdu, China, in 2010. Before he joined the School of Chemical and Biomedical Engineering at Nanyang Technological University (NTU), Singapore, he worked as a Research Engineer for RFIC Design with the VIRTUS Integrated Circuit Design Laboratory, Singapore, from 2010 and 2011, where he is currently a Post-Doctoral Researcher. His research

interests include micro/nanosolid-state biosensor, electrofluidics, acoustofluidics, optofluidics sensor and actuator, nano-electromagnetics, microwave cytometry. He also serves as the reviewer of many reputable journals such as, *IEEE Transactions* and *Lab on a Chip*.



ZHI CHEN received the B.Eng, M.Eng., and Ph.D. degrees in electrical engineering from University of Electronic Science and Technology of China (UESTC), Chengdu, China, in 1997, 2000, and 2006, respectively, where he joined the National Key Laboratory of Science and Technology on Communications, in 2006, and is currently a Professor. He was a Visiting Scholar with the University of California, Riverside, CA, USA, from 2010 to 2011. His current research interests include

wireless communication and signal processing, microwave communication, and THz communication. He has served as a reviewer for various international journals and conferences, including *IEEE Transactions on Vehicular Technology* and *IEEE Transactions on Signal Processing*.



YONG-LING BAN received the B.S., M.S., and Ph.D. in mathematics from Shandong University, Jinan, China, in electromagnetics from Peking University, Beijing, China, and in microwave engineering from the University of Electronic Science and Technology of China (UESTC), Chengdu, China, in 2000, 2003, and 2006, respectively. In 2006, he joined the Institute of Xi'an Mechanical and Electrical Information, Xi'an, China, from China North Industries Group Corporation, Beijing, China, as a Microwave Engineer. He moved to Huawei Technologies Company, Ltd., in Shenzhen, China, first as a RF Antenna Design Engineer and then as a Senior Design Engineer. In Huawei, he designed and implemented various antennas for 15 data card and mobile phone products customized from leading telecommunication industries such as Vodafone. Since 2010, he has been an Associate Professor with the Department of Microwave Engineering, UESTC. His research interests

include wideband small antenna for 3G/LTE handheld and mobile devices, directional patch antennas and arrays for mobile small base station, MIMO antenna decoupling techniques, and nano antenna.



YUEJUN KANG received the Ph.D. degree in mechanical engineering from Vanderbilt University, Nashville, TN, USA, in 2008. He was a Post-Doctoral Researcher with Monash University, Clayton, VIC, Australia, and Los Alamos National Laboratory, Los Alamos, NM, USA. Then, he joined the School of Chemical and Biomedical Engineering, Nanyang Technological University, Singapore, as an Assistant Professor in 2011. His research are fundamental understanding of

micro/nanofluidics, and leverage these understanding towards the frontier lab-on-a-chip technologies to address critical and challenging questions in diagnostics, therapeutics, tissue engineering and regenerative medicine, and bio-energy and environmental studies. His current research focus includes microfluidic biosensors and environmental sensors, cells-on-a-chip, on-chip tissue engineering, and therapeutic microdevices.